

UC Davis

UC Davis Previously Published Works

Title

Study of Čerenkov Light Emission in the Semiconductors TlBr and TlCl for TOF-PET

Permalink

<https://escholarship.org/uc/item/4954k6t4>

Journal

IEEE Transactions on Radiation and Plasma Medical Sciences, 5(5)

ISSN

2469-7311

Authors

Arino-Estrada, Gerard

Roncali, Emilie

Selfridge, Aaron R

et al.

Publication Date

2021-09-01

DOI

10.1109/trpms.2020.3024032

Peer reviewed



HHS Public Access

Author manuscript

IEEE Trans Radiat Plasma Med Sci. Author manuscript; available in PMC 2022 September 01.

Published in final edited form as:

IEEE Trans Radiat Plasma Med Sci. 2021 September ; 5(5): 630–637. doi:10.1109/trpms.2020.3024032.

Study of Čerenkov Light Emission in the Semiconductors TlBr and TlCl for TOF-PET

Gerard Ariño-Estrada [Member, IEEE],

Department of Biomedical Engineering, University of California at Davis, Davis, CA 95616 USA.

Emilie Roncali [Senior Member, IEEE],

Department of Biomedical Engineering, University of California at Davis, Davis, CA 95616 USA.

Aaron R Selfridge,

Biomedical Engineering Department, University of California, Davis, CA 95616 USA. He is now with United Imaging America, Houston, TX 77054, USA.

Junwei Du [Senior Member, IEEE],

Department of Biomedical Engineering, University of California at Davis, Davis, CA 95616 USA.

Jaroslav Glodo,

Radiation Monitoring Devices, Inc., Watertown, MA 02472, USA.

Kanai S. Shah,

Radiation Monitoring Devices, Inc., Watertown, MA 02472, USA.

Simon R. Cherry [Fellow, IEEE]

Department of Biomedical Engineering, University of California at Davis, Davis, CA 95616 USA.

Abstract

Thallium bromide (TlBr) and thallium chloride (TlCl) are semiconductor materials with high transparency to visible light, high index of refraction, and high detection efficiency for gamma rays and annihilation photons. This manuscript reports on measurements of the light intensity and timing response of Čerenkov light emitted in one 3 mm × 3 mm × 5 mm slab of each of these materials operated in coincidence with a lutetium fine silicate (LFS) crystal with dimensions of 3 mm × 3 mm × 20 mm. A ^{22}Na radioactive source was used. The measured average number of detected photons per event was 1.5 photons for TlBr and 2.8 photons for TlCl when these materials were coupled to a silicon photomultiplier. Simulation predicts these results with an overestimation of 12%. The best coincidence time resolution (CTR) for events in TlBr and TlCl were 329 ± 9 ps and 316 ± 9 ps, respectively, when events with 4 photons and >7 photons were selected. Simulation showed the CTR degraded from 120 ps to 405 ps in TlCl, and from 160 ps to 700 ps in TlBr when the first or second Čerenkov photon were selected. Results of this work show TlCl has a stronger Čerenkov light emission compared to TlBr and a greater potential to obtain the best timing measurements. Results also stress the importance of improving detection efficiency and transport of light to capture the first Čerenkov photon in timing measurements.

Keywords

TOF-PET; Fast timing; γ ray; TlBr; TlCl; CCI Detectors

I. INTRODUCTION

IMAGE quality in time-of-flight positron emission tomography (TOF-PET) improves significantly with the timing resolution of the detectors [1], [2], [3]. Recent studies report on substantial improvements in timing resolution by using high-frequency and low-noise readout electronics [4] [5] to read out fast scintillators and γ ray emitter materials, such as lutetium oxyorthosilicate (LSO) or bismuth germanate (BGO), with single or dual-ended readouts [6] [7] [8]. Lead fluoride (PbF_2) has also been used as a pure γ ray emitter coupled to microchannel plate photomultipliers (MCP-PMT) to achieve coincidence time resolutions below 50 ps full width at half maximum (FWHM) [9, 10]. The best reported CTR to date is of 30 ps FWHM using a γ ray emitter at the entrance of the MCP-PMT [11]. While improving timing resolution attracts most of the interest in the development of TOF-PET detectors, good energy resolution and depth-of-interaction (DOI) resolution remain equally important in applications such as preclinical imaging, brain imaging, dynamic imaging in regions with very low uptake, or cell tracking studies [12]. In these applications, the reduced field-of-view (FOV) or lower statistics increase the importance of applying an efficient scatter event rejection process, defining the line-of-response (LOR) very accurately, and using a radiation background-free material.

γ ray charge induction (CCI) detectors have been recently proposed as a choice that combines very good timing, energy, and spatial resolution performance [13]. CCI detectors consist of semiconductor materials that are also γ ray emitters, such as thallium bromide (TlBr). A CCI TlBr device operated in coincidence with a reference detector achieved a coincidence time resolution (CTR) of 330 ps FWHM by reading out the γ ray light. It is expected that CCI TlBr detectors achieve an energy resolution comparable to state-of-the-art TlBr devices only using charge induction readout, namely $\sim 1.5\%$ at 662 keV [14]. Arrays with 1 mm pixel pitch have shown DOI accuracy down to 1 mm [15]. A potential limitation of CCI TlBr detectors for TOF-PET is the limited number of ~ 10 γ ray photons that are produced within its transparent range [16] for 511 keV gamma depositions. This low number results primarily from the relatively high cut-off wavelength of 440 nm, due to the TlBr bandgap energy of 2.56 eV. Most of the γ ray light is emitted in the near-ultraviolet, therefore, reducing this cut-off wavelength would increase the transmission of γ ray light significantly.

Thallium chloride (TlCl) is a semiconductor material with physical properties close to those of TlBr (Table I). TlCl has a similar density and effective atomic number for 511 keV photons but a wider bandgap than TlBr, which directly translates into less absorption of visible light thus allowing more γ ray photons to be transported to the photodetector, see Fig. 1. This makes TlCl a good candidate material to improve the detection efficiency and timing properties of CCI detectors. It is also expected to show comparable charge drift properties to TlBr based on the relatively similar crystal lattice structure and bandgap.

The aim of this work is to study the light emission and transport properties of TlCl compared to TlBr in terms of timing performance and light intensity. Two slabs of TlBr and TlCl were operated each in coincidence with a lutetium fine silicate (LFS)-SiPM reference detector to evaluate their timing performance. In parallel, we developed a Monte Carlo simulation using GATE V8 [17] and compared results to TlBr experimental data. Simulations have also been conducted with TlCl to estimate the β - γ light output and results were compared to experimental data.

II. MATERIALS AND METHODS

A. TlBr and TlCl samples

One sample of TlBr and one sample of TlCl were provided by Radiation Monitoring Devices, Inc. (RMD, Watertown, MA). Both samples had dimensions of $3 \times 3 \times 5 \text{ mm}^3$. All crystal faces in each slab were lapped with a #600 grit SiC slurry and the $3 \times 3 \text{ mm}^2$ faces of each slab were also polished with a 3 micron grit slurry. The crystals were then chemically etched in a 2% bromine in methanol solution. Both slabs were wrapped with Teflon, leaving only one of the $3 \times 3 \text{ mm}^2$ faces uncovered. Optical grease (BC-630, Saint-Gobain, Courbevoie, France) was used to couple the uncovered faces to the SiPM.

B. Coincidence Acquisition Setup

Figure 2 depicts the coincidence acquisition setup used. An LFS crystal with dimensions of $3 \times 3 \times 20 \text{ mm}^3$ coupled to a S140160–3050 SiPM with $3 \times 3 \text{ mm}^2$ active area (Hamamatsu Photonics KK, Hamamatsu, Japan) was used as a reference detector. The SiPM was read out with a custom front-end printed circuit board (PCB) with a high-frequency readout circuit based on the work described in reference [4], see Fig. 3. This readout produces two signal outputs, one optimized for timing measurements and another for energy measurements. The TlCl and TlBr slabs were coupled to another S14160–3050 SiPM. The setup was kept in a metallic enclosure at a temperature of 20°C . The SiPMs were biased at 42.0 V, corresponding to an overvoltage of 4 V. The signals were recorded using a DRS4 Evaluation Board (Paul Scherrer Institute, Villigen, Switzerland) with a sampling rate of 5 Gs/s and a record length of $\sim 200 \text{ ns}$. The DRS4 was set to trigger on coincidences between the timing channels of the reference detector and the β - γ detector (Ch1 and Ch3 in Fig. 2). Trigger thresholds were set to -450 mV and -30 mV respectively, when either the TlCl or TlBr crystals were coupled. The timing resolution of the reference detector was measured separately using a second identical LFS crystal. A ^{22}Na source with an activity of $\sim 330 \text{ kBq}$ was used for all the measurements.

C. Amplitude Measurement

Both the energy and timing signals of the reference detectors were recorded to trigger the coincidence circuitry on 511 keV events, and calculate the coincidence timing spectrum and CTR.

The SiPM dark count spectrum was measured at 20°C , an overvoltage of 4V, and without any crystal attached. The DRS4 evaluation board was set to trigger on individual events and the trigger threshold was set to -15 mV .

The energy of the reference detector was measured through the maximum of the energy output. The light intensity in the TlBr and TlCl crystals was measured through the amplitude of their timing signals. No energy output was recorded when the light in TlBr and TlCl was detected, as the expected signal was expected to be too weak to provide any meaningful information.

D. CTR Measurement

The timing outputs were used to evaluate the CTR in all configurations. The CCI detector timing signal was delayed by ~ 1 ns with respect to the reference detector. The time pick off was done using leading edge discrimination with a multiscale approach based on a coarse and a fine threshold. This approach is critical to precisely estimate the γ emission time stamps while minimizing the effect of noise, as the γ emission is very fast and the limited number of photons results in waveforms with low amplitude.

A coarse threshold was set to -450 mV and -30 mV, for the reference and TlBr/TlCl detectors, respectively. For each waveform, the first point of the curve with a value greater than the coarse threshold was selected and referred to as coarse timestamp. A fine threshold was set to -60 mV and -2 mV for the reference and TlBr/TlCl detectors, respectively. Leading edge threshold was applied starting 50 positions before the coarse timestamp. The first point in that range with a value greater than the fine threshold was selected and referred to as fine timestamp. Interpolation was used between the fine timestamp and the previous point to obtain the final timestamp.

To calculate the CTR FWHM, the distribution of coincidence detection times was interpolated to find the time points corresponding to half the maximum amplitude. The uncertainty on the FWHM was estimated by combining the squared distance between the interpolated half maximum time and the two closest neighbors in the true distribution, for both the upper and lower values.

E. GATE Simulation

Simulations were conducted with a 511 keV monoenergetic source directed at a detector composed of a $3 \times 3 \times 5$ mm³ TlBr or TlCl crystal coupled to an S14160–3050 SiPM (Hamamatsu, Japan). A total of 75,000–80,000 photoelectric events were collected in the detector depending on the configuration. Compton events were not considered in this study, as they are typically removed from coincidence timing resolution measurements for TOF-PET.

1) Generation and transport of γ photons in GATE v8.0—GATE simulations were conducted in TlBr and TlCl crystals. The crystal optical properties were defined by the index of refraction and absorption length. The index of refraction was defined as a function of wavelength [16] [17], while the absorption length was modelled as a step function (equal to zero below the cut-off wavelength and infinitely large above the cut-off).

The index of refraction affects the number of γ photons produced in a material according to the Frank-Tamm formula [24], so the γ yield is also wavelength dependent.

The generation of the Čerenkov photons in GATE is done through Geant4 [26]. Secondary electrons are emitted when a 511 keV annihilation photon interacts with the semiconductor. Čerenkov photons may be emitted along the path of the electron with a momentum determined by the kinetic energy and momentum of the parent electron, and the index of refraction of the material [27]. The photons are then transported in the crystal, reflecting from the faces or being internally absorbed. The self-absorption in TlBr and TlCl is different based on their bandgap levels, as illustrated in Fig. 4(right) by the vertical lines. The interaction of the Čerenkov photons with the crystal faces were modelled in GATE V8.0 with the LUT Davis model [17]. LUTs describing TlBr and TlCl surfaces covered with Teflon tape were used on all five faces of the crystal not in contact with the SiPM. The exit face was modelled as a polished surface coupled to the SiPM with optical grease (index of refraction 1.5), assumed to have 100% transparency for Čerenkov photons.

Multiple characteristics such as detection time (time of crystal-photodetector interface crossing), travel time in the crystal, 3D coordinates of the final position and momentum, and energy were saved for all detected photons. The number of generated Čerenkov photons for each gamma interaction was also recorded. The photon detection efficiency (PDE) of the SiPM was modelled based on the manufacturer datasheet: above 30% above 300 nm with a maximum value of 60% at 450 nm corresponding to an overvoltage of 4V.

2) Coincidence Timing Resolution—Each coincidence event timing was characterized by the time pick-off values from the pair of gamma interactions in each detector. For each gamma interaction, the time pick-off was defined as the first or second photon detection time. This allows calculation of the best timing resolution for different time pickoff values. The coincidence timing spectrum was obtained by subtracting the timing pick-off values from each detector and histogramming the differences. The CTR was extracted from each spectrum as the FWHM. The timing spectrum was also characterized by the full width at tenth maximum (FWTM).

III. RESULTS

A. SiPM Dark Count Spectrum

Figure 5 shows the spectra of dark count events acquired with the SiPM. The trigger threshold was set at -15 mV. Peaks represent events with an increasing number of microcells triggering. Peaks for one, two, and three cells were clearly distinguishable and evenly spaced by ~ 20 mV, and the peak for four cells can also be discerned although the statistics are low. One can appreciate some shoulders on the right-side of the peaks, especially for the single-cell case. Those are likely due to after-pulse effects.

B. Characterization of reference detectors

Figure 6 shows the CTR of two identical LFS reference detectors for events with 511 keV energy depositions on both detectors. The measured FWHM of the detection time distribution was 217 ps. The single timing resolution was estimated as $217/\sqrt{2} = 153$ ps.

C. TlBr and TlCl light intensity comparison

1) Measurements—Figure 7 shows the light intensity (signal amplitude in V) spectra for TlBr and TlCl. The trigger threshold was set to 30 mV to reject dark count events with one cell triggering. Consequently, events with a single detected photon were rejected as well. Only coincidences with an energy deposition of 511 keV in the reference detector were selected for the intensity analysis. Both spectra show clearly the peaks for 2, 3, and 4 photons, although the relative peak heights were very different for each dataset. Figure 8 shows the number of events with 2, 3, 4, and 5 photons for the datasets shown in Fig. 7. The number of photons per event was determined according to the divisions shown in Fig. 7. Each dataset was fitted to a Poisson distribution such that $P(k) = C \lambda^k \exp(-\lambda) / k!$, where k was the number of detected photons. The expected value for each distribution, λ , was 1.52 and 2.78, for the TlBr and TlCl distributions, respectively.

2) Simulation of scintillation photon emission and detection—Figure 9 shows the distribution of the number of emitted scintillation photons for ~75,000 simulated photoelectric events in the TlBr and TlCl crystals. The distribution exhibited a Gaussian shape, with a mean of 11.9 emitted photons for TlBr between 440 nm- 800 nm, which is in agreement with our previous simulations [16]. In comparison, TlCl produced 58% more photons, with an average of 18.9 photons between 380 nm and 800 nm. 82% more photons were detected with TlCl than TlBr (expectation of 3.1 photons and 1.7 photons following a Poisson distribution of photon numbers), making the material more attractive for timing resolution. For both materials, the number of detected photons predicted by the simulations was ~12% higher than what was estimated by the experiments (1.52 photons for TlBr and 2.78 photons for TlCl), which may be explained by the absence of Compton events as well as a simplified model of the SiPM that does not account for its geometrical efficiency and timing properties. The lower cutoff wavelength of TlCl (380 nm vs. 440 nm for TlBr) allows for the transmission of scintillation photons in a spectral band where the PDE is greater than 50% and reaches its maximum of 60% (Fig. 4 (right)). These photons will therefore be more likely detected by the SiPM thus contributing to the greater detection efficiency than that of TlBr.

D. TlBr and TlCl CTR Measurement

Figure 10 shows the CTR for the TlBr and TlCl datasets for events with a given number of detected photons. Amplitude cuts were made according to the divisions depicted in Fig. 7. Figure 11 shows the timing spectra for TlBr events with 4-photons (left) and TlCl events with >7-photons (right), corresponding to the best CTR.

E. Analysis of Timing Properties Using Simulated Data

The detection times for all first and second detected photons were histogrammed for TlBr and TlCl (Fig. 12). The distributions showed an early peak followed by a slow decay, indicating that most photons were detected in a short period of time. The first photon distributions have peaks at 42 ps and 35 ps for TlBr and TlCl, respectively. As expected, the second detected photons were delayed with respect to the first photons, with a distribution peak at 63 ps and 56 ps for TlBr and TlCl, respectively. TlCl showed a sharper distribution

than TlBr for both first and second photons (81% and 52% of photons detected in 0.1 ns, vs 68% and 38% for TlBr), which suggests that TlCl can achieve better time resolution. The detection times are composed of the scintillation emission time and the travel time in the crystal. In contrast to scintillators with slow light emission, scintillation photons are emitted within a few picoseconds after the secondary electron is produced, which makes the detection times almost identical to the travel time in the crystal. This travel time is caused by the multiple reflections of the photons at the crystal boundaries including the exit face in contact with the photodetector. Improving the travel time by optimizing the transport and extraction of the scintillation photons can play an important role in improving the detector timing resolution [28].

For each material, the coincidence timing spectra were calculated with a time pick off on the first or second detected photon (Fig. 13). All spectra showed a Lorentzian shape, consistent with the scintillation emission [4] [28] [29]. Using a Lorentzian fit, the CTR FWHM was found to be 160 ps and 120 ps for TlBr and TlCl when triggering on the first photon, Fig. 13 (left). As a comparison (not shown here), when including all scintillation photons assuming a PDE of 1, the 1st photon CTR was 100 ps and 60 ps for TlBr and TlCl, respectively. The strong effect of the PDE is associated with the very low number of scintillation photons emitted per photoelectric event, ranging between 11 and 19 depending on the material (Fig. 9) and was even stronger when triggering on the 2nd photon: the CTR dropped from 700 ps to 260 ps for TlBr and from 405 ps to 140 ps for TlCl when assuming a PDE of 1.

IV. DISCUSSION

Scintillation light properties in TlBr and TlCl have been studied with a low-noise and high-frequency front-end circuit. Time properties of scintillation luminescence in a TlBr crystal were studied previously [13],[16], however, this work deepens our understanding through measurements and simulations of light intensity and timing properties in TlBr. This work also reports for the first time on the timing and intensity properties of scintillation light produced in TlCl and compares the performance with TlBr.

Light intensity measurements showed an event count rate over 5 times greater in TlCl than in TlBr. Simulations overestimated the average number of detected photons per event by 12%. That overestimation is consistent in both the TlBr and TlCl datasets. Despite having a lower index of refraction, TlCl effectively results in more scintillation light detection than TlBr due to the much shorter cut-off wavelength. The ratio of 2-photon events in TlBr and TlCl was of $\sim 3x$ in real data (Fig. 7) and of $\sim 2x$ in simulations (Fig. 9). That discrepancy could be attributed to the presence of scattered events in the real data that are not present in the simulation.

Timing measurements with TlBr agreed with those reported previously. No timing measurements with TlCl were previously reported. CTR values for TlCl were consistently greater than those of TlBr for events with 1, 2, and 3 detected photons. This is attributed that to the greater fraction of scattered events in the TlCl sample. As TlCl has a greater scintillation light yield than TlBr, it is more likely that scattered events generate a detectable signal in

TlCl. The deterioration of CTR values for 5 and 6 photons per event in the TlBr dataset is attributed to the lack of statistics.

The best measured CTR was 329 ps and 316 ps for TlBr and TlCl (Fig. 11). These are higher than the CTR values predicted by the simulations, which did not include the photodetector time response and noise. For example, the 1st photon CTR for TlCl coupled to a photodetector with a 90 ps transit time spread would be 157 ps.

Simulation results showed the second scintillation photons arrive at the photodetector approximately 20 ps on average after the first one. CTRs worsened from 120 to 405 ps in TlCl and from 160 ps to 700 ps when selecting only the first or second scintillation photons. This effect could be mitigated by i) improving the light collection through improved photodetector efficiency, ii) improving the light transport and extraction to reduce the transit time spread in the crystal and ensuring that the detector can trigger on the earliest photon, or iii) correct the detection time based on DOI estimation.

Recent studies report on CTRs below 50 ps FWHM when scintillation emitters such as lead glass or PbF₂ are coupled to MCP-PMTs [10][11], which suggests events with very few optical photons have the capacity to provide timing resolutions well below the >300 ps FWHM reported in this manuscript. The difference in timing performance between the aforementioned studies and the present one can be explained by the superior SPTR and signal-to-noise ratio of MCP-PMTs compared to SiPMs. Therefore, it suggests an appropriate photodetector choice could lead to much better timing resolutions in TlBr and TlCl without compromising detection efficiency. This hypothesis should be evaluated with future studies.

V. CONCLUSIONS

Scintillation light production in TlCl is only 60% greater than in TlBr but provides a dramatically increased detection rate and timing accuracy. This shows small improvements of the brightness in scintillation crystals with low light yields or scintillation emitters can lead to much better performance.

TlCl is a semiconductor material and can be used to manufacture competitive CCI detectors as it presents better timing and detection efficiency properties than TlBr. TlCl detectors with charge induction readout need to be tested to prove its feasibility to be used as a CCI device. CCI detectors can show simultaneous outstanding performance in timing, energy, and spatial resolution. Events with 511 keV energy, selected using the charge induction signal, are expected to show a larger average number of detected scintillation photons per event than in the results presented in this work and, therefore, improve timing properties. Moreover, their 3-D segmentation capabilities could be used to estimate the DOI and correct the transit time within the crystal to further improve timing accuracy. If proven successful, CCI TlCl detectors would be an excellent choice for TOF-PET, as well as for prompt gamma imaging in quality assurance in proton therapy.

ACKNOWLEDGMENTS

This work was supported by NIH grants R35 CA197608 (PI Cherry), R01 EB027130 (PI Roncali), R03 EB025533 (PI Ariño-Estrada), and R21 EB028398 (PI Ariño-Estrada). The authors would like to thank Hamamatsu Photonics K.K. for providing the SiPM samples, and Dr. Javier Caravaca for helpful discussions.

REFERENCES

- [1]. Surti S, "Update on time-of-flight PET imaging," *J. Nucl. Med.*, vol. 56, no. 1, pp. 98–105, 1.2015. [PubMed: 25525181]
- [2]. Surti S, and Karp JS, "Advances in time-of-flight PET," *Phys. Med.*, vol. 32, no. 1, pp. 12–22, 1. 2016. [PubMed: 26778577]
- [3]. Vanderberghe S, Mikhaylova E, D'Hoe E, Mollet P, and Karp JS, "Recent development in time-of-flight PET," *EJNMMI Physics*, vol. 3, no. 3, 2. 2016.
- [4]. Cates JW, Gundacker S, Auffray E, Lecoq P, and Levin CS, "Improved single photon time resolution for analog SiPMs with front end readout that reduces influence of electronic noise," *Phys. Med. Biol.*, vol. 63, 185022, 9. 2018.
- [5]. Gundacker S, Martinex Turtos S, Auffray E, Paganoni M, and Lecoq P, "High-frequency SiPM readout advances measured coincidence time resolution limits in TOF-PET," *Phys. Med. Biol.*, vol. 64, 055012, 2. 2019.
- [6]. Kwon SI, Roncali E, Gola A, Paternoster G, Piemonte C, and Cherry SR, "Dual-ended readout of bismuth germinate to improve timing resolution in time-of-flight PET," *Phys. Med. Biol.*, vol. 64, 105007, 2019.
- [7]. Cates JW, and Levin CS, "Electronics method to advance the coincidence time resolution with bismuth germanate," *Phys. Med. Biol.*, vol. 64, 175016, 2019.
- [8]. Gundacker S, Martinez Turtos S, Kratochwil N, R Hendrika Pots M. Paganoni P. Lecoq, and E. Auffray, "Experimental time resolution limits of modern SiPMs and TOF-PET detectors exploring different scintillators and Cherenkov emission", *Phys. Med. Biol.*, vol. 65, 025001, 2020.
- [9]. Korpar S, Dolenc R, Križan P, Pestotnik R, and Stankovnik A, "Study of TOF-PET using Cherenkov light", *Physics Procedia*, vol. 37, pp.1531–1536, 2012.
- [10]. Ota R, Nakajima N, Hasegawa T, Ogawa I, and Tamagawa Y, "Timing-performance evaluation of Cherenkov-based radiation detectors", *NIM A*, vol. 923, pp. 1–4, 2019.
- [11]. Ota R, Nakajima K, Ogawa I, Tamagawa Y, Shimoi H, Suyama M, and Hasegawa T, "Coincidence time resolution 30 ps FWHM using pair of Cherenkov-radiation-integrated MCT-PMTs," *Phys. Med. Biol.*, vol. 64, 07LT01, 2019.
- [12]. Man F, et al., "In Vivo PET Tracking of ^{89}Zr -Labeled V γ 9V62 T Cells to Mouse Xenograft Breast Tumors Activated with Liposomal Alendronate," *Molecular Therapy*, vol. 27 no. 1, pp. 219–28, 2019. [PubMed: 30429045]
- [13]. Ariño-Estrada G, Mitchell G, Kim H, Du J, Kwon SI, Cirignano LJ, Shah KS, and Cherry SR, "First Cherenkov Charge Induction (CCI) TIBr Detectors for TOF-PET and Proton Range Verification," *Phys. Med. Biol.*, vol. 64 175001, 2019.
- [14]. Kim H, "Thallium Bromide Gamma-Ray Spectrometers and Pixel Arrays," *Front. Phys.*, vol. 8 55, 2020.
- [15]. O'Neal S, Koehler W, He Z, Kim H, Cirignano L, and Shah K, "Characterization of a digital ASIC readout system for 11 \times 11 pixelated TIBr detectors," *IEEE Nucl. Sci. Symp. Med. Im. Conf.*, 2014.
- [16]. Ariño-Estrada G, Mitchell G, Kwon SI, Du J, Kim H, Cirignano LJ, Shah KS, and Cherry SR, "Towards time-of-flight PET with a semiconductor detector," *Phys. Med. Biol.*, vol. 63 04LT01, 2018.
- [17]. Stockhoff M, Jan S, Dubois A, Cherry SR, Roncali E, "Advanced optical simulation of scintillation detectors in gate v8.0L First implementation of a reflectance model based on measured data," *Phys. Med. Biol.*, vol. 62 L1–L8, 2017. [PubMed: 28452339]

- [18]. Lide DR, "Handbook of Chemistry and Physics," 100th Edition. [Online]. Available: <http://http://www.hbcponline.com/faces/contents/ContentsSearch.xhtml>
- [19]. Schröter H, "Über die Brechungsindizes einiger Schwermetallhalogenide im Sichtbaren und die Berechnung von Interpolationsformeln für den Dispersionsverlauf (On the refractive indices of some heavy-metal halides in the visible and calculation of interpolation formulas for dispersion)," Z. Phys, vol. 67 pp. 24–36, 1931.
- [20]. Palik ED, Handbook of Optical Constants of Solids, Academic Press., Boston, MA, USA, 1985.
- [21]. Owens A, Compound semiconductor radiation detectors, CRC Press., Boca Raton, FL, USA, 2016.
- [22]. Lewellen TK, "The challenge detector designs for PET," AJR. Am. J. Roentgenol, vol. 195 no. 2, pp. 301–09, 2010. [PubMed: 20651184]
- [23]. Berger MJ, Hubbell JH, Seltzer SM, Chang J, Coursey JS, Sukumar R, Zucker DS, and Olsen K, XCOM: Photon Cross Section Database (version 1.5). [Online] National Institute of Standards and Technology, Gaithersburg, MD, USA. Apr. 2020. Available: <http://physics.nist.gov/xcom>.
- [24]. Wojtowicz AJ, Drozdowski W, Wisniewski D, Lefaucheur J-L, Galazka Z, Gou Z, Lukasiewicz T, Kisielewski J, "Scintillation properties of selected oxide monocrystals activated with Ce and Pr," Optical Materials, vol. 28 pp. 85–93, 2006.
- [25]. Cherry SR, Sorenson JA, Phelps ME, Physics in Nuclear Medicine, 4th ed. W.B. Saunders., Philadelphia, PA, USA, pp. 87–106, 2012.
- [26]. Agostinelli S, et al., Geant4: a simulation toolkit Nucl. Instrum. Methods. A., vol. 506 pp.250–303, 2003.
- [27]. Jelley JV, "Cerenkov Radiation and its Applications," Br. J. App. Phys. vol. 6 227, 1955.
- [28]. Roncali E, Kwon SI, Jan S, Berg E, and Cherry SR, "Cerenkov light transport in scintillation crystals explained: Realistic simulation with gate," Biom. Phys. Express. vol. 5, 2019.
- [29]. S Brunner and D. Schaart, "Enabling cost-effective TOF-PET by exploiting the Cherenkov emission in BGO", J. Nucl. Med, vol. 58150, 2017.



Fig. 1.
(Left) Photograph of a TlBr ingot. (Right) Photograph of a TlCl ingot wrapped with Teflon tape.

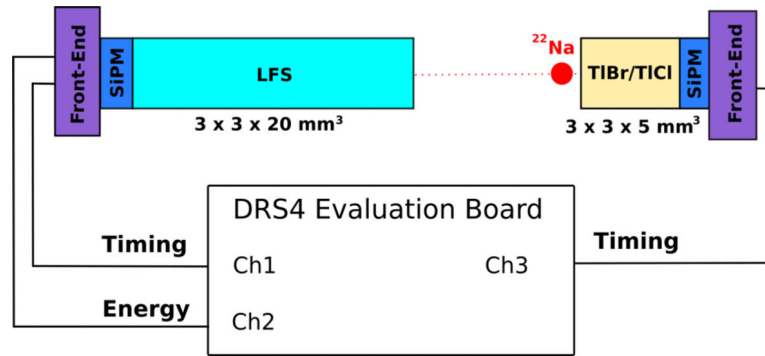


Fig. 2. Acquisition setup with the LFS reference detector operated in coincidence with the TlBr or TlCl detector.

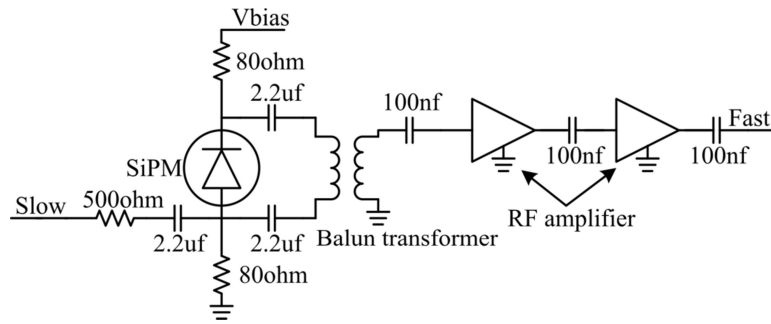


Fig. 3.
Schematic of the PCB used to read out the SiPMs.

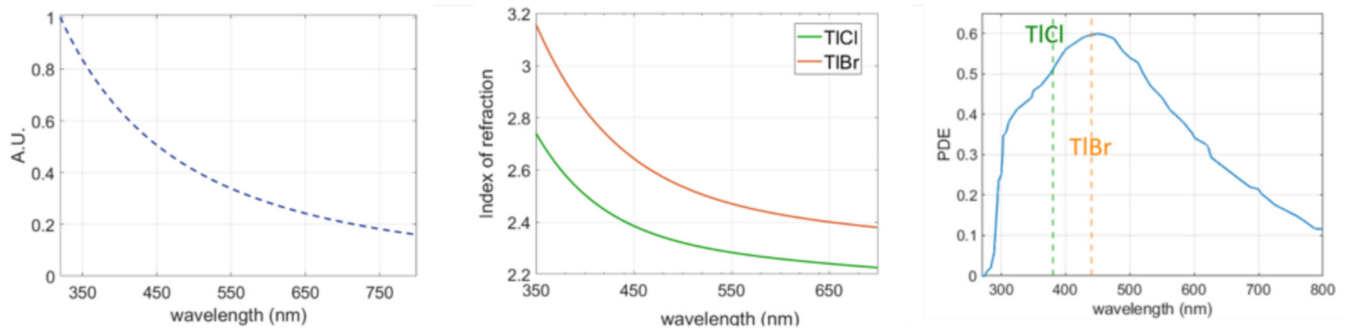


Fig. 4.

TlBr and TlCl material characteristics. (Left) The Cerenkov emission spectrum is inversely proportional to the square of the wavelength. (Center) The wavelength-dependent index of refraction for TlBr and TlCl affects the generation of the Cerenkov photons, their absorption, and reflections on the crystal faces. For both materials, the index varies by $\sim 30\%$ over the spectrum considered, indicating the importance of modelling the wavelength dependency. (Right) The SiPM PDE reaches a maximum at 0.6 at 450 nm. The green and orange lines indicate the cutoff wavelengths for TlCl and TlBr, respectively.

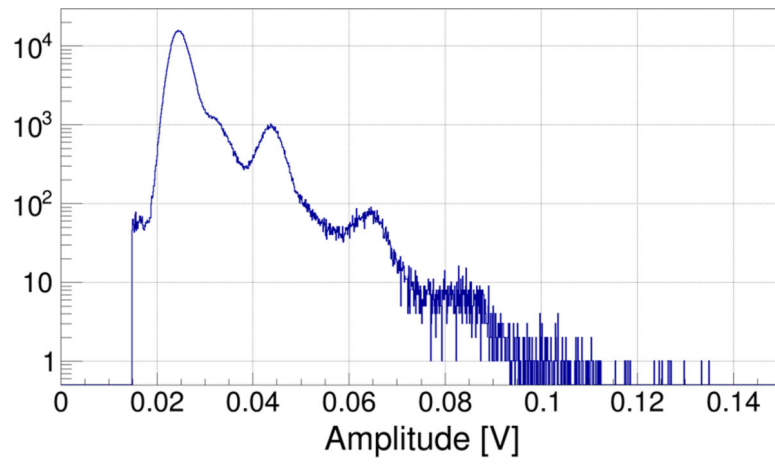


Fig. 5. Experimental data. Dark count spectra of the SiPM operated at 42 V bias voltage and at room temperature (20°C).

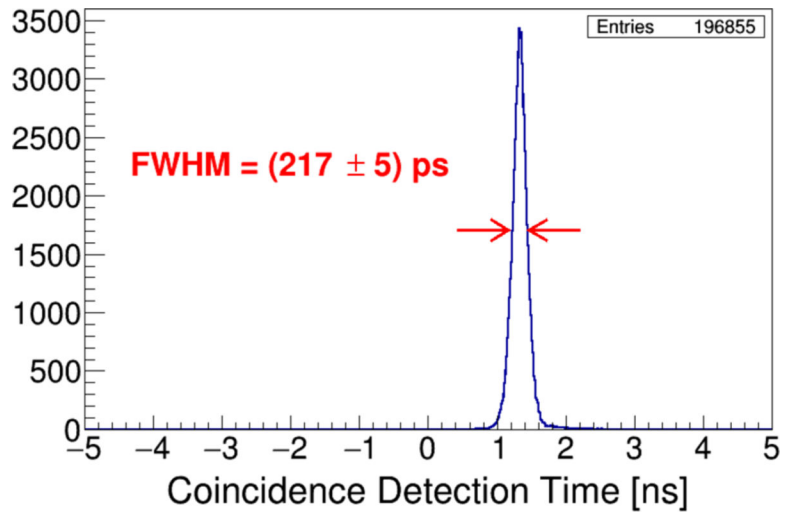


Fig. 6. Experimental data. CTR of two identical reference detectors. Events with 511 keV energy only were included in the datasheet.

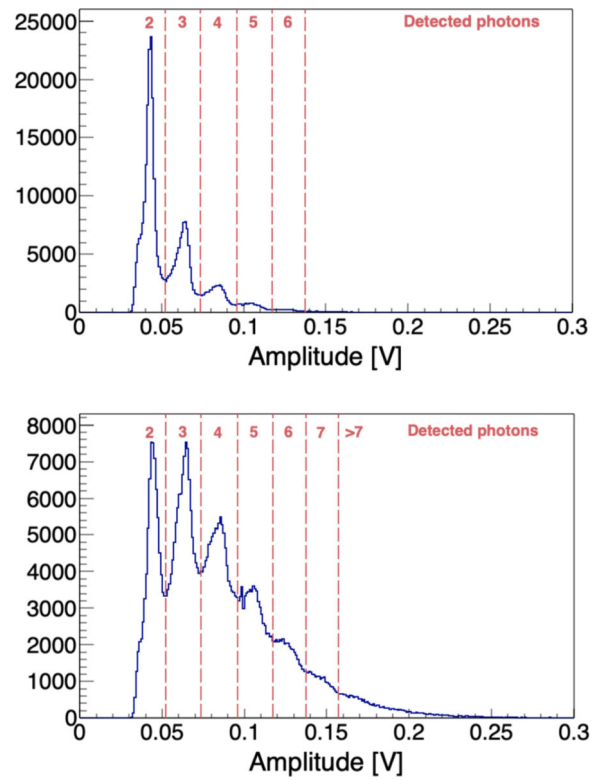


Fig. 7. Experimental data. Light intensity distributions of events in top) TlBr, and bottom) TlCl. Both distributions show discrete peaks corresponding to the detected photons individually.

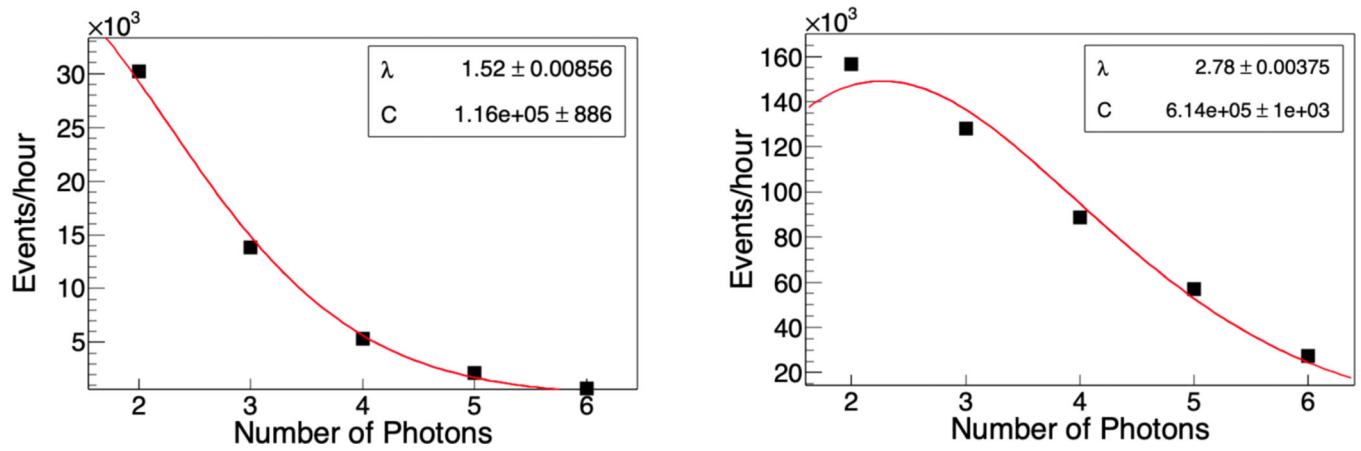


Fig. 8. Experimental Data. Distribution of events with a given number of detected photons for TIBr (left), and TICl (right). Error bars inside markers.

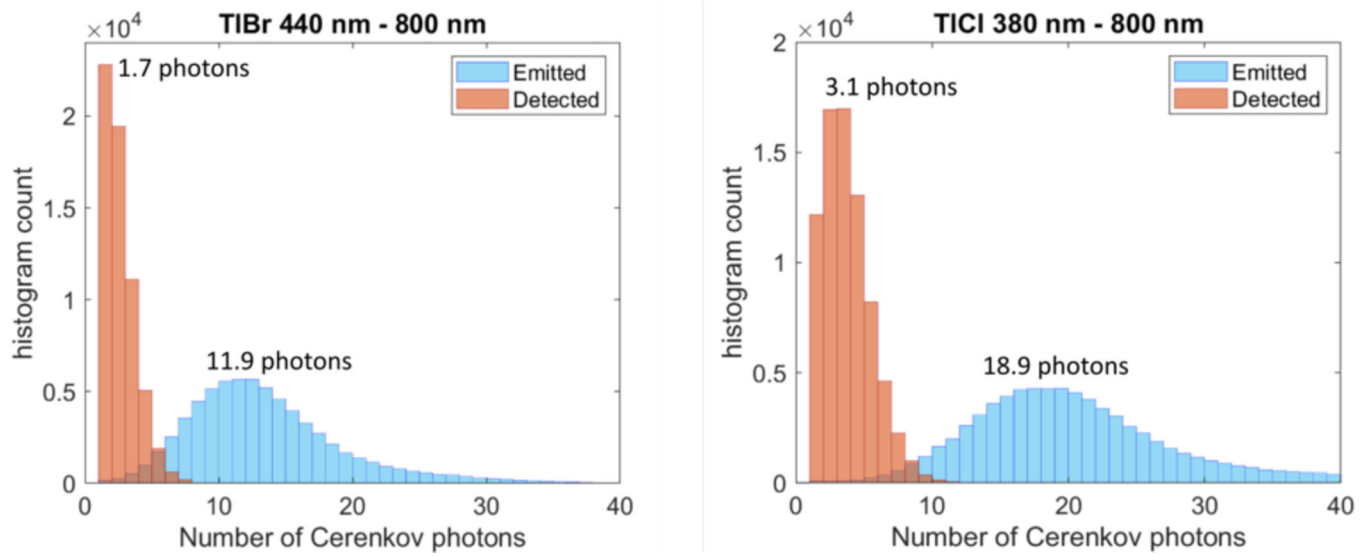


Fig. 9. Simulation. Distribution of emitted and detected Cerenkov photons from simulation for TIBr (left) and TlCl (right). The average number of emitted photons was 11.9 and 18.9 photons, respectively. Only a fraction of those photons are detected (accounting for the PDE), with an expectation of 1.7 photons and 3.1 photons for TIBr and TlCl, respectively.

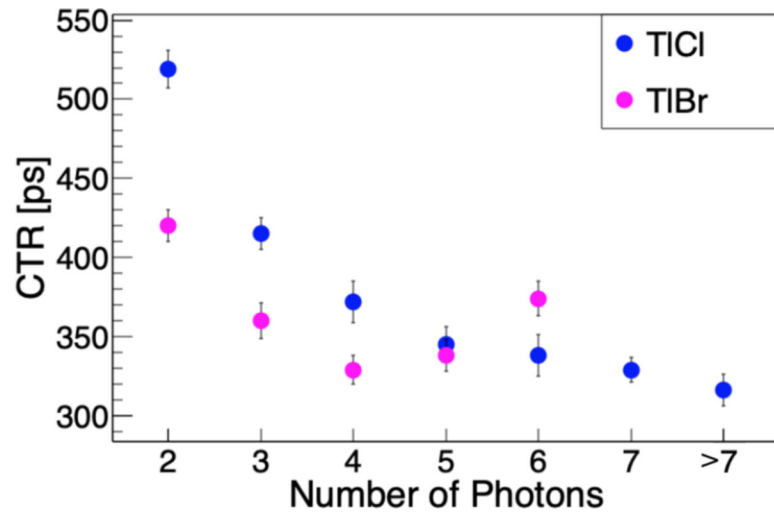


Fig. 10. Experimental data. CTR for TIBr and TICI datasets vs number of photons per event.

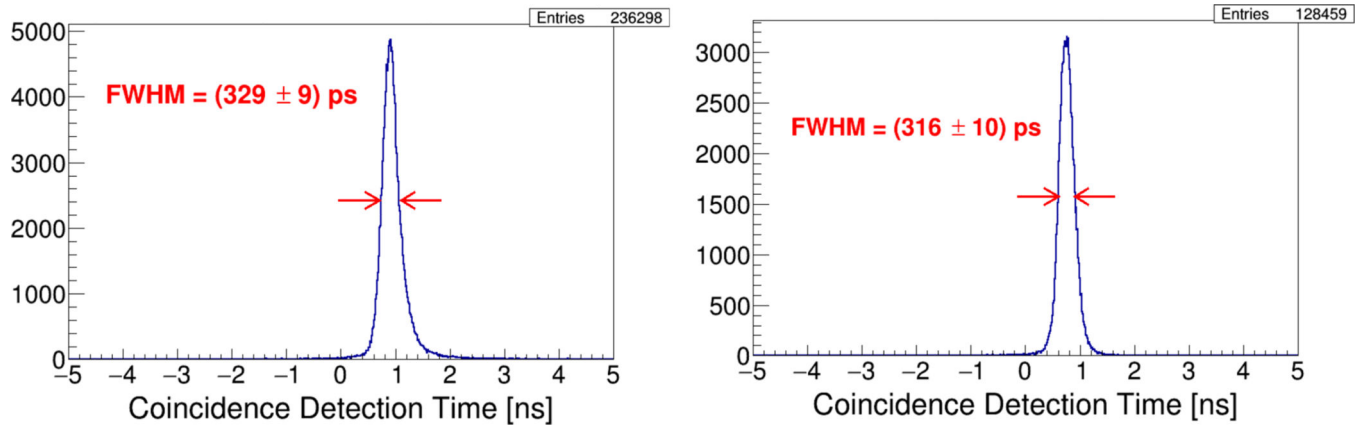


Fig. 11. Experimental data. (Left) CTR for TlBr events with 4 detected photons. (Right) CTR for TlCl events with >7 detected photons.

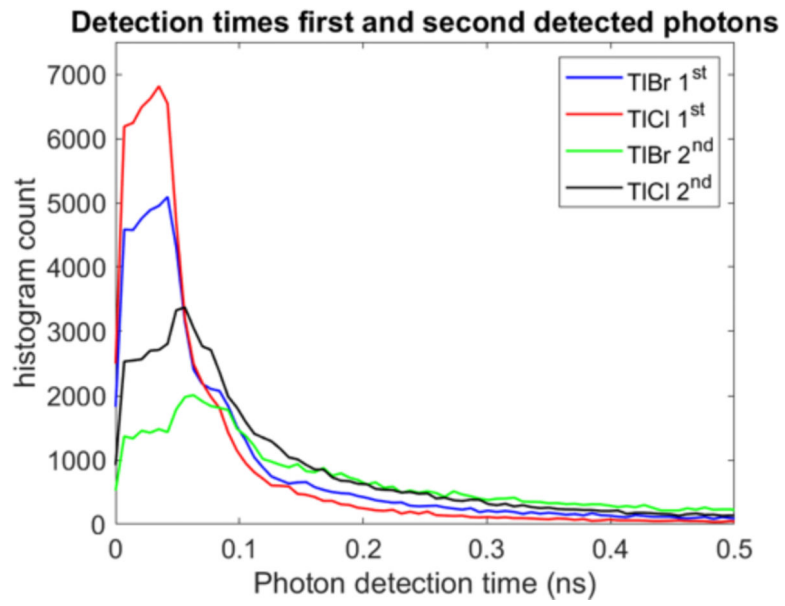


Fig. 12. Simulation. Distribution of the detection times when only the first or second γ photon arriving at the SiPM surface is detected.

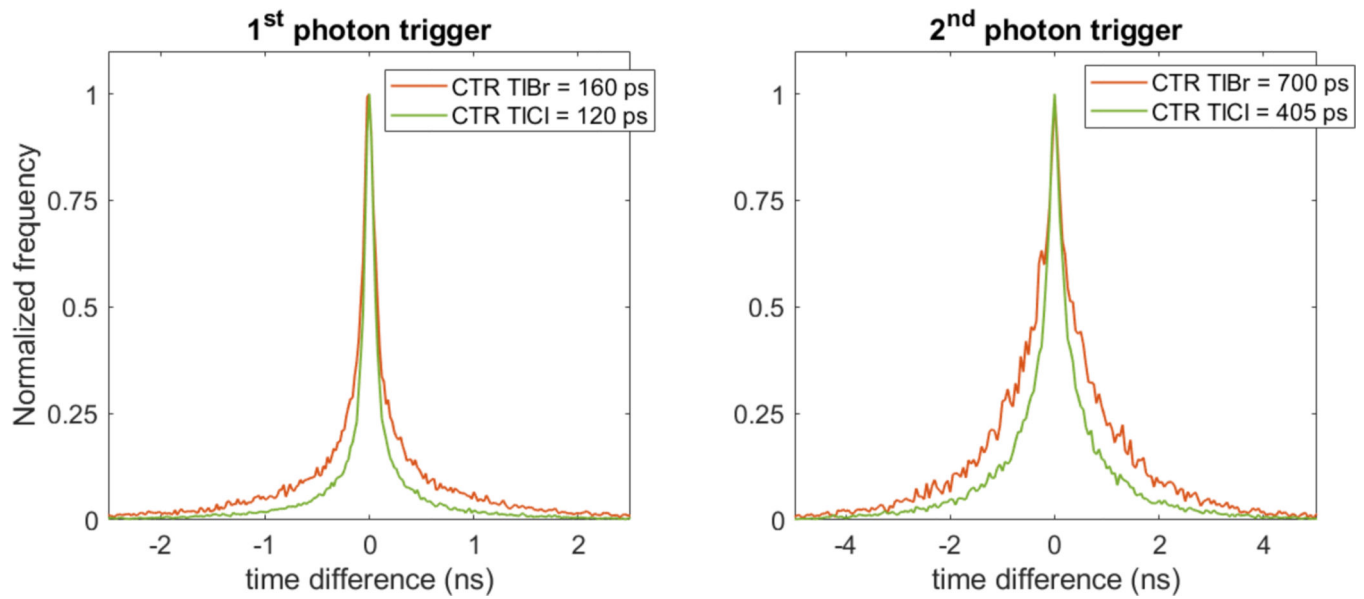


Fig. 13. Simulation. Coincidence timing spectra for first and second detected photon time pickoff (left and right, respectively), showing a Lorentzian shape, consistent with the bremsstrahlung emission. TICI has a better CTR than TIBr for both time pickoff as indicated in the legend.

TABLE I**PHYSICAL PROPERTIES OF LSO, BGO, TLBR, AND TLCL**

Symbol	LSO	BGO	TlBr	TlCl
Density [g/cm ³]	7.4	7.1	7.5	7.0
Z_{eff} 100 – 600 keV	66	73	74	77
Attenuation length for 500 keV [cm]	1.15	1.09	0.97	0.97
500 keV photofraction [%]	33	42	43	46
Index of refraction (at 570 nm)	1.8	2.1	2.6	2.3
Cutoff wavelength [nm]	~180	320	440	380
Melting point (°C)	2050	1050	460	431

Data from [18], [19], [20], [21], [22], [23], [24]. Effective atomic number evaluated according to [25]. Photofraction has been evaluated as the cross-section of 500 keV photoelectric interactions over total cross section.

Author Manuscript

Author Manuscript

Author Manuscript

Author Manuscript